

LOCUSS: THE MASS DENSITY PROFILE OF MASSIVE GALAXY CLUSTERS AT Z=0.2

NOBUHIRO OKABE¹, GRAHAM P. SMITH², KEIICHI UMETSU¹, MASAHIRO TAKADA³, AND TOSHIFUMI FUTAMASE⁴
Draft version August 23, 2018

ABSTRACT

We present a stacked weak-lensing analysis of an approximately mass-selected sample of 50 galaxy clusters at $0.15 < z < 0.3$, based on observations with Suprime-Cam on the Subaru Telescope^{1,2}. We develop a new method for selecting lensed background galaxies from which we estimate that our sample of red background galaxies suffers just 1% contamination. We detect the stacked tangential shear signal from the full sample of 50 clusters, based on this red sample of background galaxies, at a total signal-to-noise ratio of $\bar{S}/N = 32.7$. The Navarro-Frenk-White model is an excellent fit to the data, yielding sub-10% statistical precision on mass and concentration: $M_{\text{vir}} = 7.19_{-0.50}^{+0.53} \times 10^{14} h^{-1} M_{\odot}$, $c_{\text{vir}} = 5.41_{-0.45}^{+0.49}$ ($c_{200} = 4.22_{-0.36}^{+0.40}$). Tests of a range of possible systematic errors, including shear calibration and stacking-related issues, indicate that they are sub-dominant to the statistical errors. The concentration parameter obtained from stacking our approximately mass-selected cluster sample is broadly in line with theoretical predictions. Moreover, the uncertainty on our measurement is comparable with the differences between the different predictions in the literature. Overall our results highlight the potential for stacked weak-lensing methods to probe the mean mass density profile of cluster-scale dark matter halos with upcoming surveys, including Hyper-Suprime-Cam, Dark Energy Survey, and KIDS.

Subject headings: galaxies: clusters: general — gravitational lensing: weak

1. INTRODUCTION

Gravitational lensing is a powerful probe of the matter distribution in galaxy clusters, because the observed signal is sensitive to the total matter distribution and insensitive to the physical processes at play within clusters. Many studies have therefore employed gravitational lensing to probe the mass and internal structure of galaxy clusters (Kneib & Natarajan 2011, and references therein). Prominent among these studies are those that aim to measure the dependence of cluster density on cluster-centric radius, i.e. the “density profile” of clusters (e.g. Miralda-Escude 1995; Smith et al. 2001; Gavazzi et al. 2003; Kneib et al. 2003; Dahle et al. 2003; Sand et al. 2004; Broadhurst et al. 2005; Limousin et al. 2007; Johnston et al. 2007; Oguri et al. 2009; Okabe et al. 2010; Umetsu et al. 2011; Oguri et al. 2012; Newman et al. 2013). A major motivation is to test key predictions from the cold dark matter theory of structure formation: (1) the density profile of the dark matter halos posited to host galaxies and cluster of galaxies is predicted to be universal and follow a simple 2-parameter model (Navarro et al. 1997),

and (2) massive galaxy cluster-scale dark matter halos have concentrations⁵ of $c_{200} \equiv r_{200}/r_s \simeq 3 - 4$ (e.g. Bullock et al. 2001; Dolag et al. 2004; Neto et al. 2007; Duffy et al. 2008; Zhao et al. 2009), and are thus “less concentrated” than less massive halos.

In order to probe the density profile across a large dynamic range, lensing studies have typically combined weak- and strong-lensing signals, and have thus been limited to small samples of strong-lensing-selected clusters. These studies typically find that strong-lensing clusters have high central concentrations in projection (e.g. Gavazzi et al. 2003; Kneib et al. 2003; Broadhurst et al. 2008; Umetsu et al. 2011; Oguri et al. 2012). Moreover, joint lensing and dynamical studies find that the density profile of the dark matter component may be shallower than predicted from cold dark matter simulations (Newman et al. 2013). Interpretation of these apparent tensions between observations and theory is complicated by possible selection biases, small sample size, lensing-projection bias caused by halo triaxiality, and the absence of baryons from the simulations upon which the predictions are based.

We adopt a complementary approach that aims to make progress on overcoming issues relating to sample size and selection, and lensing projection biases. Building on earlier stacked lensing studies (Dahle et al. 2003; Johnston et al. 2007; Okabe et al. 2010; Umetsu et al. 2011; Oguri et al. 2012, hereafter Ok10,), we measure the mean density profile of massive clusters by stacking the weak-lensing signal from a sample of 50 approximately mass-selected clusters. Our sample comprises *all* clusters from the *ROSAT* All Sky Survey catalogs

¹ Academia Sinica Institute of Astronomy and Astrophysics (ASIAA), P. O. Box 23-141, Taipei 10617, Taiwan; okabe@asiaa.sinica.edu.tw

² School of Physics and Astronomy, University of Birmingham, Edgbaston, Birmingham, B15 2TT, UK; gps@star.sr.bham.ac.uk

³ Kavli Institute for the Physics and Mathematics of the Universe (Kavli IPMU, WPI), The University of Tokyo, Chiba 277-8582, Japan

⁴ Astronomical Institute, Tohoku University, Aramaki, Aoba-ku, Sendai, 980-8578, Japan

⁵ Based in part on observations obtained at the Subaru Observatory under the Time Exchange program operated between the Gemini Observatory and the Subaru Observatory.

² Based in part on data collected at Subaru Telescope and obtained from the SMOKA, which is operated by the Astronomy Data Center, National Astronomical Observatory of Japan.

⁵ r_{200} is the radius within which the mean density is $200\times$ the critical density of the universe, and r_s is a “scale radius” at which $d \log \rho / d \log r = -2$.

(Ebeling et al. 1998, 2000; Böhringer et al. 2004) that satisfy $L_X[0.1 - 2.4\text{keV}]/E(z)^{2.7} \geq 4.2 \times 10^{44} \text{ erg s}^{-1}$, $0.15 \leq z \leq 0.30$, $n_H < 7 \times 10^{20} \text{ cm}^{-2}$, and $-25^\circ < \delta < +65^\circ$, where $E(z) \equiv H(z)/H_0$ is the normalized Hubble expansion rate, and selecting on $L_X/E(z)^{2.7}$ mimics a mass selection (Popesso et al. 2005). We stress that our results are based on the *full sample* of 50 clusters; subsamples of clusters will be discussed in future articles.

In Section 2 we describe our data and analysis; in Section 3 we explain our results and compare with numerical simulations; and in Section 4 we summarize our conclusions. We use the concordance Λ CDM model of $\Omega_{M,0} = 0.27$, $\Omega_\Lambda = 0.73$ and $H_0 = 100h \text{ km s}^{-1} \text{ Mpc}^{-1}$ (Komatsu et al. 2011). In this cosmology the virial over-density at the mean redshift of our cluster sample, $\langle z \rangle = 0.23$ is $\Delta_{\text{vir}} = 113.77$. All error bars are 68% confidence intervals unless otherwise stated.

2. SUBARU DATA AND WEAK-LENSING ANALYSIS

We observed all 50 clusters with Suprime-Cam (Miyazaki et al. 2002) on the Subaru Telescope, as part of the Local Cluster Substructure Survey (LoCuSS⁶) – 46 clusters through the V/i' -band filters; two each through the V/I_C - and g/i' -band filters. Hereafter we refer to the bluer filter as V and the redder filter as i' . The full-width half maximum of point sources in the V/i' bands is $0''.6 \lesssim \text{FWHM} \lesssim 0''.9$ and $0''.5 \lesssim \text{FWHM} \lesssim 0''.7$, respectively. Photometric calibration to $\leq 10\%$ precision in both filters was achieved via observations of Landolt standard stars, and double checked against SDSS/DR8 stellar photometry (Eisenstein et al. 2011).

We measure the shape of faint galaxies using a modified version of Ok10’s pipeline, based on the IMCAT⁷ (Kaiser et al. 1995, hereafter, KSB). The main modification is to calibrate the KSB isotropic correction factor for individual objects using galaxies detected with high significance $\nu > 30$ (Umetsu et al. 2010). This minimizes the inherent shear calibration bias in KSB+ methods in the presence of measurement errors (Okura & Futamase 2012).

We define a sample of background galaxies based on color with respect to the red sequence of early-type galaxies in each cluster. In principle selecting red galaxies ($\Delta C \equiv (V - i') - (V - i')_{\text{ES0}} > 0$) yields a clean sample of background galaxies. In reality a positive color cut is required to eliminate contamination by faint red cluster galaxies due to statistical errors and possible intrinsic scatter in galaxy colors (e.g. Broadhurst et al. 2005). In contrast, interpretation of “blue galaxy” ($\Delta C < 0$) samples is complicated by star-formation. For completeness, we include blue galaxies in this section, however our results in Section 3 are based only on the red galaxy sample.

The mean tangential distortion strength averaged over (1) all galaxies satisfying each color cut, (2) cluster-centric radii of $0.1 h^{-1} \text{ Mpc} < r < 2.8 h^{-1} \text{ Mpc}$, and (3) all 50 clusters, $G_+ \equiv \langle \langle g_+ \rangle \rangle$, increases monotonically with ΔC for red galaxies (Fig. 1). We interpret the steep slope at $0 \lesssim \Delta C \lesssim 0.3$ as arising from contamination by cluster members. Indeed, the mean cluster-

centric radius of red galaxies is an increasing function of ΔC at small ΔC (Fig. 1). At $\Delta C \gtrsim 0.4$ we interpret the shallow slope of G_+ as arising from a slowly increasing redshift of the faint red background population as ΔC increases. We therefore model the data with a Gaussian of width σ centered at $\Delta C = 0$ (to represent the cluster population), and the mean lensing kernel, $D(\Delta C) \equiv \langle D_{ls}/D_s \rangle$, for galaxies in the COSMOS photometric redshift catalog (Ilbert et al. 2009) that matches each color cut. The model for the color-dependence of G_+ is therefore: $G_+(\Delta C) = AD(\Delta C)(1 - Bf(\Delta C))$, where A converts D into shear in a simple manner, B is the normalization of the Gaussian contaminant function at $\Delta C = 0$, and $f(\Delta C > 0) = [1 - \text{erf}(\Delta C/\sqrt{2}\sigma)]/2$. This model has three free parameters: A , B , and σ , and allows to estimate explicitly the fraction of contaminant galaxies, f , as a function of ΔC .

The best-fit model describes the red galaxies well (Fig. 1, upper panel). We conservatively adopt a limit of 1% on contaminating fraction, which translates into a red color cut of $\Delta C > 0.475$. We select galaxies redder than this cut for the results presented in Section 3; the mean number density of these galaxies is $5.3 \pm 1.9 \text{ arcmin}^{-2}$ per cluster, where the uncertainty is the standard deviation among the 50 clusters. We therefore achieve a total stacked number density of red galaxies of $266.3 \text{ arcmin}^{-2}$.

For completeness, we applied the same methods to blue galaxies, describing the contaminating fraction as $f(\Delta C < 0) = [1 + \text{erf}(\Delta C/\sqrt{2}\sigma)]/2$. The model does not describe the blue galaxies well, and we do not use them in Section 3.

3. RESULTS

Our results are based on stacking the *red* background galaxy sample, defined by $\Delta C > 0.475$ (Section 2), for *all* 50 clusters in the sample.

3.1. Stacking and Modeling the Weak Shear Signal

We detect each individual cluster at a typical peak signal-to-noise ratio of $S/N \simeq 4$ in two-dimensional Kaiser & Squires (1993) mass reconstructions. We also stack the shear catalogs in physical length units centered on the respective BCGs and reconstruct the average cluster mass distribution for the *full* sample, with a peak signal-to-noise ratio of $S/N = 28$ (Fig. 2). Motivated by the symmetrical average mass map, we constructed the stacked tangential shear profile for the full sample (Fig. 3) following the procedure of Umetsu et al. (2011). In brief, we center the catalogs on the respective BCGs, and stack in physical length units across the radial range $100 h^{-1} \text{ kpc} < r < 2.8 h^{-1} \text{ Mpc}$, in 14 log-spaced bins. We detect the signal at $S/N = 32.7$, using the full covariance matrix to take into account projected uncorrelated large-scale structure and intrinsic ellipticity noise (e.g. Hoekstra 2003; Hoekstra et al. 2011; Oguri & Takada 2011; Umetsu et al. 2011; Oguri et al. 2012), computing the cosmic-shear contribution using the non-linear matter power spectrum (Smith et al. 2003) for the WMAP7 cosmology and the shape noise from the diagonal matrix. The 45° -rotated distortion component is consistent with a null signal, confirming that residual systematic errors are at least an order of magnitude smaller than the measured lensing signal.

⁶ <http://www.sr.bham.ac.uk/locuss>

⁷ <http://www.ifa.hawaii/kaiser/IMCAT>

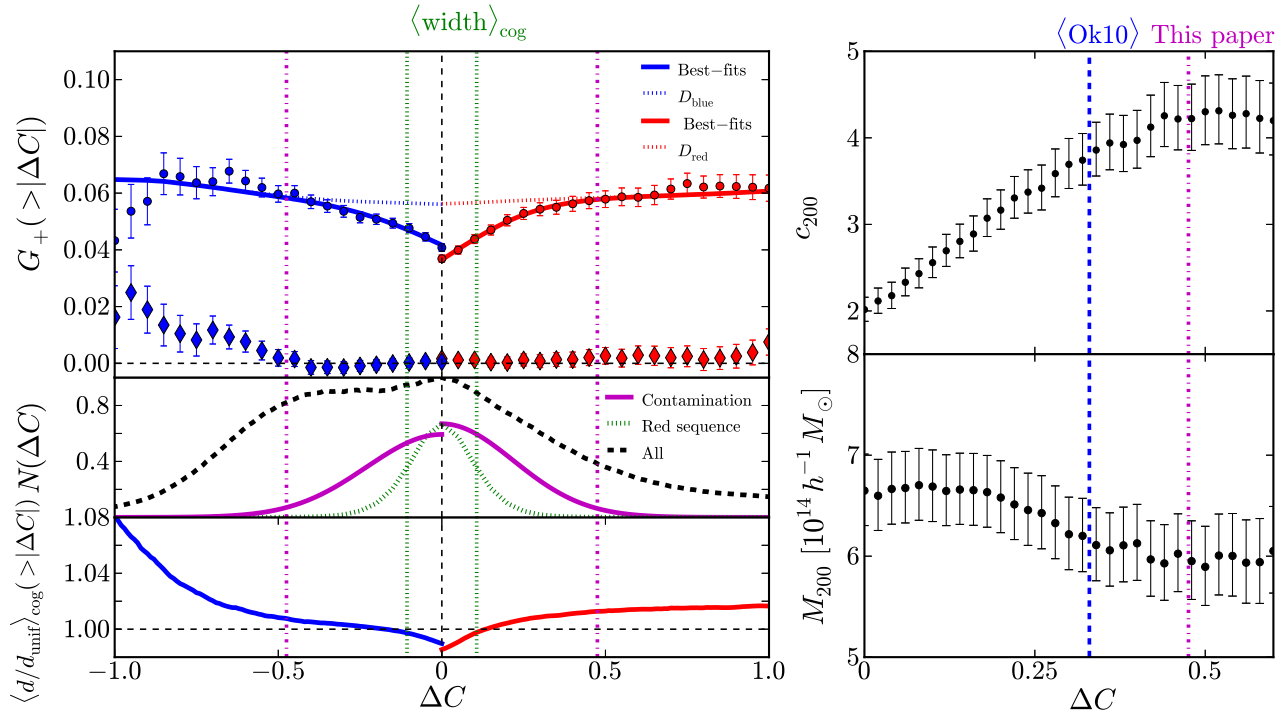


FIG. 1.— TOP-LEFT: Stacked reduced shear G_+ (Section 2) as a function of color offset from the stacked cluster red sequence (filled circles). Filled diamonds show the mean shear calculated after rotating galaxies through 45° . Solid curves show the best-fit lensing kernel plus contamination model described in Sec 2. The vertical dashed-dotted line shows the color cut at which the fraction of contaminants is 1%. MIDDLE-LEFT: The color distribution of all galaxies at $21 < i' < 26$ (black dashed curve). The width of the red sequence of bright ($i' < 20$) cluster members is shown as the green dotted curve, with the green vertical lines de-marking the 1σ width of the red sequence. The magenta curves show the color distribution of contaminants in our model, and upon which the 1% contamination cut is based. The faint blue population appears to be preferentially found at large cluster centric radii, suggesting that blue galaxy contamination may be dominated by galaxies in the cluster outskirts. RIGHT: The run of c_{200} (upper) and M_{200} (lower) with ΔC , showing the color cut that we adopt in this paper (magenta dot-dashed) and that of Ok10 (blue dashed). Ok10 (see their Figure 14) chose their color cuts by eye based on the mean tangential distortion strength for the cluster sample.

TABLE 1
DENSITY PROFILE MODELS

Model	Shape parameter ^a	M_{vir} ($10^{14} h^{-1} M_\odot$)	c_{vir}^b	M_{200} ($10^{14} h^{-1} M_\odot$)	c_{200}^b	$\chi^2_{\text{min}}/\text{d.o.f}$
NFW	$\gamma = 1$	$7.19^{+0.53}_{-0.50}$	$5.41^{+0.49}_{-0.45}$	$5.98^{+0.40}_{-0.38}$	$4.22^{+0.40}_{-0.36}$	7.2/12
gNFW	$\gamma = 1.27^{+0.24}_{-0.37}$	$7.50^{+0.74}_{-0.65}$	$4.88^{+0.86}_{-0.86}$	$6.15^{+0.48}_{-0.44}$	$3.79^{+0.69}_{-0.69}$	6.6/11
Einasto	$\alpha = 0.188^{+0.062}_{-0.058}$	$7.49^{+0.86}_{-0.73}$	$4.92^{+0.57}_{-0.80}$	$6.15^{+0.50}_{-0.45}$	$3.82^{+0.48}_{-0.66}$	6.6/11

^a Parameter describing the shape of the mass density profile on small scales.

^b NFW-like concentration parameter defined by $c_{\Delta}^{\text{NFW}} = r_{\Delta}/r_s$, $c_{-2}^{\text{gNFW}} = (r_{\Delta}/r_s)/(2-\gamma)$ and $c_{\Delta}^{\text{Einasto}} = r_{\Delta}/r_{-2}$.

The stacked shear profile (Fig 3) is well-described by the so-called NFW profile: $\rho \propto x^{-1}(1+x)^{-2}$, where $x \equiv r/r_s$, and $d \log \rho / d \log r = -2$ at $r = r_s$ (Navarro et al. 1997). We express our model fits in terms of the virial mass $M_{\text{vir}} \equiv (4\pi/3)\rho_{\text{cr}} \Delta_{\text{vir}} r_{\text{vir}}^3$, and the concentration parameter $c_{\text{vir}} \equiv r_{\text{vir}}/r_s$, where Δ_{vir} is the virial overdensity and ρ_{cr} is the critical density. We measure both parameters to sub-10% statistical precision (Table 1), obtaining a best fit concentration parameter of $c_{\text{vir}} = 5.4 \pm 0.5$. Indeed, the statistical errors on concentration are comparable with the differences between the predictions from different numerical simulations (Fig. 3). Moreover the observed concentration parameter exceeds the predicted concentration from numerical simulations

(Duffy et al. 2008; Zhao et al. 2009; Bhattacharya et al. 2011; De Boni et al. 2012).

The NFW model fit described above does not motivate fitting more flexible models to our data (Table 1). Nevertheless, for completeness, we fit the generalized NFW (gNFW) and Einasto (1965) profiles. The former adds a free parameter γ to the NFW profile: $\rho \propto x^{-\gamma}(1+x)^{-3+\gamma}$; the latter describes the shape of the profile slope thus: $d \log \rho / d \log r = -2(r/r_{-2})^\alpha$. The best-fit gNFW profile is consistent with NFW, with $\gamma = 1.27^{+0.24}_{-0.37}$. The best-fit Einasto profile has $\alpha = 0.19 \pm 0.06$, consistent with numerical simulations, e.g. $\langle \alpha \rangle = 0.175 \pm 0.046$ (Gao et al. 2012), and $\langle \alpha \rangle = 0.183$ (Navarro et al. 2004). We also measure the inner slope

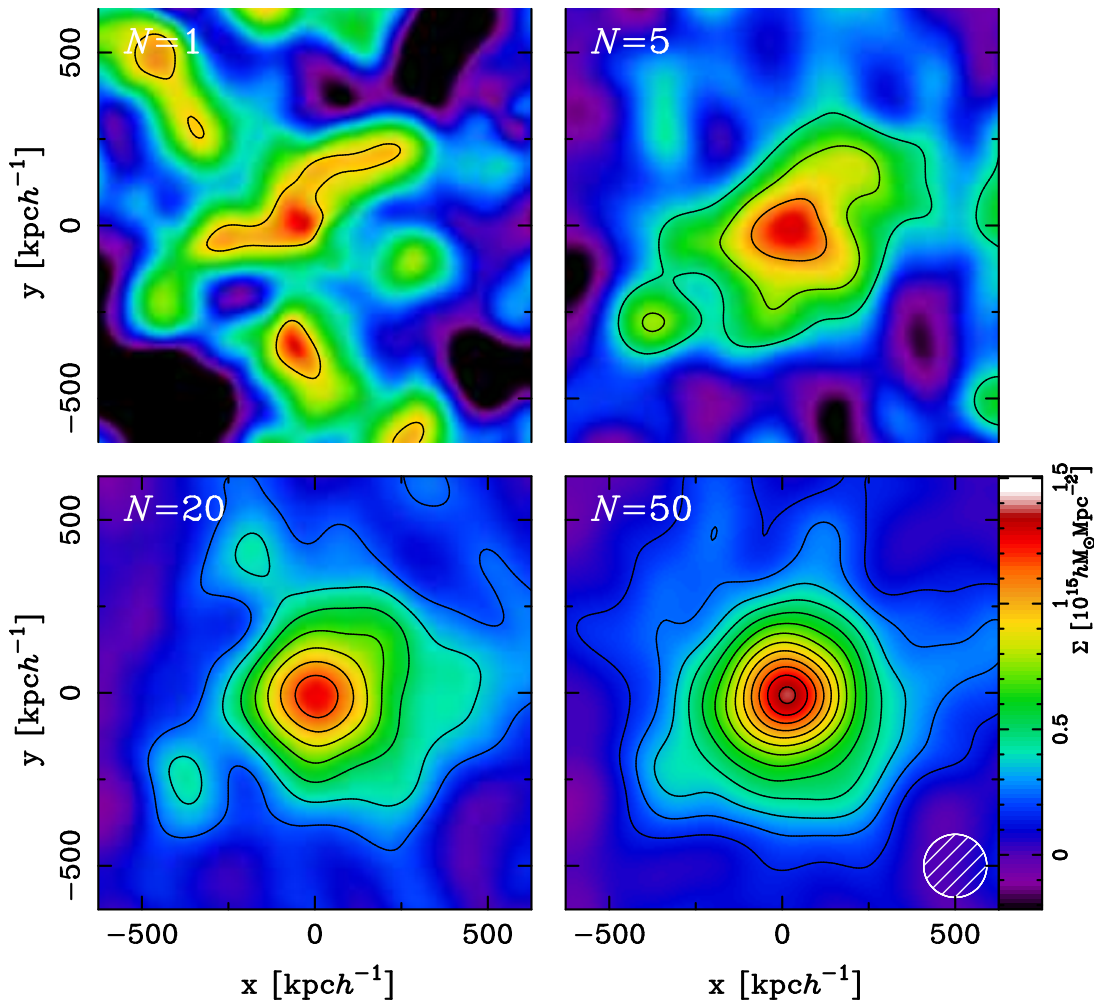


FIG. 2.— The projected mass distribution reconstructed from our weak-lensing catalogs, from one typical cluster ($N = 1$; ABELL 0141; upper left) to the full sample ($N = 50$; bottom right). Contours start at $S/N = 3$, and are spaced at $\Delta S/N = 2$. A Gaussian smoothing scale of $\text{FWHM} = 2$ arcmin is used in all panels (hatched region at lower right).

of the best fit density profile models directly, obtaining $\beta(r = 0.01r_{200}) = -d \log \rho / d \log r = 1.1$ for the gNFW and Einasto models, in good agreement with $\langle \beta \rangle \simeq 1.1$ (Navarro et al. 2004; Gao et al. 2012).

We also examine the possible impact of adiabatic contraction on the total measured density profile (e.g. Gnedin et al. 2004) by introducing a central point mass into the model. We obtain an upper limit on the point mass of $M_{\text{point}} \lesssim 12 \times 10^{12} h^{-1} M_{\odot}$, which is degenerate with the structural parameters of the smooth component in all models (NFW, gNFW, and Einasto). The best-fit mass and concentration parameters do not change significantly from those listed in Table 1. The excellent fit of the NFW model – that is based on numerical dark matter only simulations – to our weak-lensing data, and the results of adding baryons to the model (albeit in a simplified form) suggest the dark matter may not suffer adiabatic contraction by baryons in the cluster core. We will return to this topic in a future article that combines strong- and weak-lensing constraints.

3.2. Systematic Errors

We investigate the sensitivity of our results to systematic errors. In summary, we conclude that systematic errors are sub-dominant to the statistical errors discussed

in Section 3.1.

Shear calibration – We confirmed the reliability of our shape measurements using simulated data that were generated using GLAFIC (Oguri 2010) with point spread functions described by the Moffat profile with a range of seeing ($0''.5 < \text{FWHM} < 1''.1$) and power indices ($3 < \beta < 12$), as described in Oguri et al. (2012). We obtain a multiplicative calibration bias (m) and additive residual shear offset (c) (defined following Heymans et al. 2006) of $|m| \lesssim 0.03$ and $|c| \lesssim 2 \times 10^{-4}$, respectively, for $\text{FWHM} \simeq 0''.7$.

Radial and color cuts – Our results change by just $\Delta c_{\text{vir}} \simeq 0.1$ when we vary the number of bins between 8 and 18, change the inner radial cut from 80 to 200 $h^{-1} \text{kpc}$ or the outer radial cut between 2.5 and 3.5 $h^{-1} \text{Mpc}$. The stability of our results under variations of the inner radial cut underlines the robustness of our new approach to selecting red galaxies, and the negligible level of $\langle \Sigma_{\times} \rangle$ noted in Section 3.1. Moreover, the constraints on concentration are stable to $\Delta c_{\text{vir}} \lesssim 0.2$ with respect to increasing the color cut beyond $\Delta C > 0.475$, and to fitting only to galaxies brighter than $i' = 25$. The constraints on M_{vir} are stable to a few per cent under the same tests (Fig. 1).

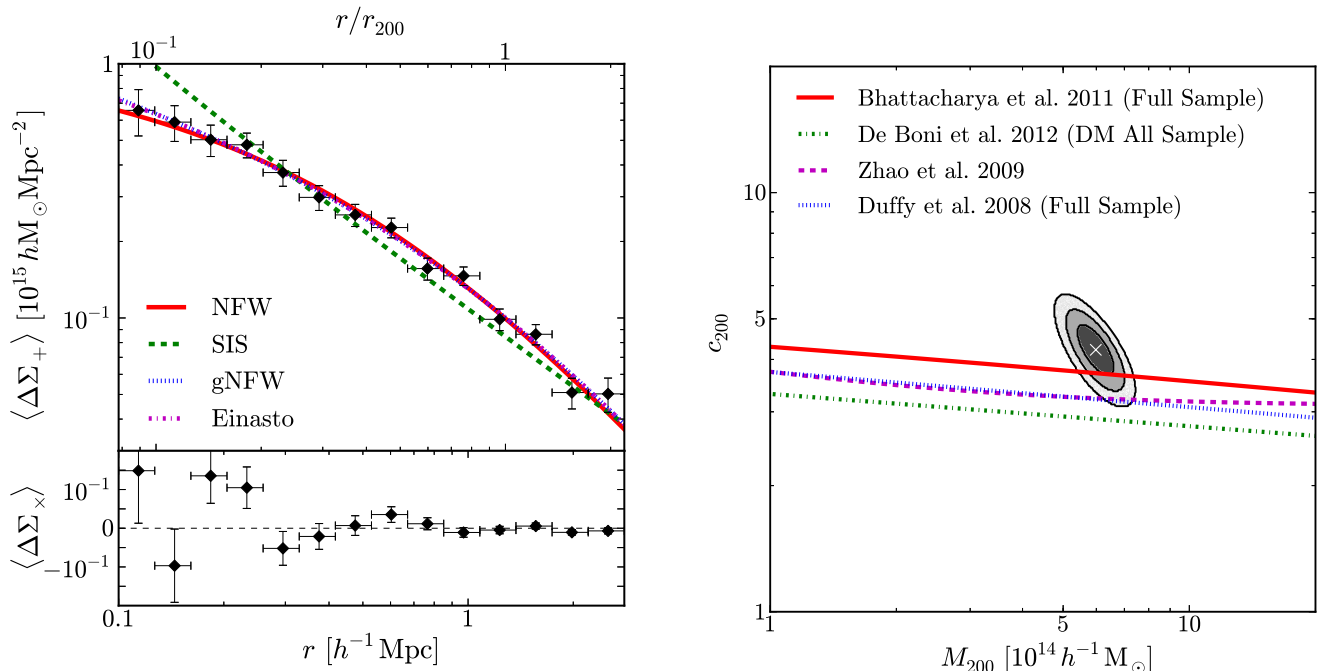


FIG. 3.— Stacked tangential shear profile of all 50 clusters in units of projected mass density, where different cluster and background galaxy redshifts galaxies are weighted by the lensing kernel (Mandelbaum et al. 2006; Okabe et al. 2010; Oguri & Takada 2011; Umetsu et al. 2011). The projected radius is computed from the weighted mean cluster redshift ($z_{\text{cluster}} \simeq 0.23$). The solid, dashed, dotted and dash-dotted curves are the best-fit Navarro-Frenk-White (NFW), singular isothermal (SIS), generalized NFW (gNFW) and Einasto profiles, respectively. The lower panel shows the result of the 45° test for systematic errors. RIGHT – Stacked weak-lensing constraints on the mass and concentration of a complete volume-limited sample of 50 galaxy clusters at $\langle z \rangle = 0.23$. The white cross denotes the best-fit parameters and the contours show the 68.3%, 95.4%, and 99.7% confidence levels. Note that the predicted relations have all been converted to be consistent with our analysis.

Stacking procedure: radial bins – We construct synthetic weak shear catalogs based on analytic NFW halos that match the mass-concentration relation predicted from numerical simulations. These catalogs match the observed number density and field of view of our Subaru data. We draw 300 samples of 50 clusters from the predicted cluster distribution, and stack the respective shear profiles in both physical length units (as in Section 3.1) and length units scaled to r_{200} of each halo. We do not detect any bias in the measured mean concentration of the stacked clusters, obtaining $\langle c/c_{\text{truth}} \rangle = 1.02 \pm 0.07$ for stacking in physical length units, and find $\langle c/c_{\text{truth}} \rangle = 1.08 \pm 0.07$ for re-scaled length units. In both cases we obtain $\langle M/M_{\text{truth}} \rangle = 0.96 \pm 0.06$; the uncertainties are the standard deviation on the 300 samples of 50 clusters. The non-detection of a systematic error arising from stacking in physical units is consistent with Ok10’s result that their mass-concentration relations from individual and stacked clusters (using physical length units) are self-consistent. We also note that stacking in re-scaled length units weights the contribution of each cluster to each bin in a nonlinear and model-dependent manner: $w \propto \theta \Delta \theta \propto r_{200}^2 \propto M_{200}^{2/3}$.

Real clusters are aspherical, embedded in the large-scale-structure, and contain baryons. As numerical hydrodynamical simulations become more realistic, robust tests based on simulated clusters should therefore become possible. We conduct a preliminary test using clusters extracted from the new “Cosmo-OWLS” simulation, that implements the AGN model described in McCarthy et al.

(2011) in a $400 h^{-1} \text{Mpc}$ box, with weak-lensing catalogs constructed following Bahé et al. (2012). The results are consistent with the analytic NFW tests – i.e. we do not detect any systematic error on the measurement of concentration based on stacking in physical length units.

Stacking procedure: centering – We also checked whether the results are affected by adopting the BCG as the center of each cluster, by adding an off-centering parameter $\sigma_{R_{\text{off}}}$ to the models following Johnston et al. (2007). The best-fit M_{vir} and c_{vir} are unchanged, and we obtain an upper limit of $\sigma_{R_{\text{off}}} < 29 h^{-1} \text{kpc}$.

3.3. Comparison with Okabe et al. (2010)

We fit an NFW model to Ok10’s stacked red+blue catalog and our own stacked red galaxy catalog for the 21 clusters in common between the two studies, finding that our mean masses and concentrations are $\sim 14 - 20\%$ and $\sim 15 - 17\%$ greater than theirs (Table 2). The main differences between Ok10 and our analysis relate to color-selection of background galaxies, and their shape measurement methods (§2). We attribute the differences between our respective mass measurements mainly to a combination of (1) contamination of Ok10’s blue galaxy sample at large cluster-centric radii and (2) systematics in Ok10’s shape measurement methods. We attribute the differences between the respective concentration measurements mainly to contamination of Ok10’s red galaxy catalog – their less conservative red color cut ($\langle \Delta C \rangle = 0.33$) leads to an overall $\sim 5\%$ contamination by galaxies that preferentially lie at small cluster-centric radii (see

TABLE 2
COMPARISON WITH OKABE ET AL. (2010)

Parameters ^a	Over-density, Δ		
	Δ_{vir}	200	500
$M_{\Delta}^{2013}/M_{\Delta}^{2010}$	1.14 ± 0.16	1.16 ± 0.14	1.20 ± 0.12
$c_{\Delta}^{2013}/c_{\Delta}^{2010}$	1.15 ± 0.19	1.16 ± 0.19	1.17 ± 0.22

^a Ratio of the stacked mass and concentration obtained from our methods and those of Ok10, for the 21 clusters in common between the two studies.

right panel of Fig. 1). We note that the results in this section are consistent with Planck Collaboration et al. (2013) and Applegate et al. (2012).

4. SUMMARY

We have used sensitive high resolution observations with Subaru to measure the average density profile of an approximately mass-selected sample of 50 galaxy clusters at $0.15 < z < 0.3$. Careful treatment of systematic errors indicates that they are all smaller than the statistical errors. In particular, we achieve just 1% contamination of the background galaxy sample by foreground and cluster galaxies, tests on simulated data indicate that our shape measurement multiplicative systematic error is $m \lesssim 0.03$, and errors from choice of binning scheme are just a few per cent. When the signal from all 50 clusters is combined together we achieve a number density of background galaxies of $266.3 \text{ arcmin}^{-2}$.

The shape of the stacked density profile is consistent with numerical simulations across the radial range $100 h^{-1} \text{ kpc} - 2.8 h^{-1} \text{ Mpc}$. Specifically, we find no statistical evidence for departures from the NFW profile. We constrain the mean mass and concentration of the clusters to sub-10% precision, obtaining $c_{\text{vir}} = 5.41^{+0.49}_{-0.45}$. This level of precision is comparable with the differences between the concentrations predicted by different numerical simulations, and therefore opens the possibility of

discriminating between different simulations using observational data in the near future.

Our results emphasize the power of stacked weak-lensing for constraining the average mass and shape of galaxy clusters. Surveys including Hyper Suprime-Cam on Subaru, the Dark Energy Survey, and KIDS, all hold much promise for stacked weak-lensing studies of less massive clusters, including those at higher redshifts. However significant advances on the precision that we have achieved here on massive low redshift clusters await future facilities such as LSST and *Euclid* to provide the required number density of background galaxies on these rare and massive low redshift clusters.

ACKNOWLEDGMENTS

We thank Ian McCarthy, Yannick Bahé, and Joop Schaye for sharing their weak shear catalogs from the Cosmo-OWLS simulation in advance of publication. We also thank our LoCuSS colleagues, especially Dan Marrone, Gus Evrard, Pasquale Mazzotta, Arif Babul, and Alexis Finoguenov for many helpful discussions and comments. We acknowledge the Subaru Support Astronomers, plus Paul May, Chris Haines, and Mathilde Jauzac, for assistance with the Subaru observations. We are grateful to N. Kaiser and M. Oguri for making their IMCAT and GLAFIC packages public. This work is supported in part by Grant-in-Aid for Scientific Research on Priority Area No. 467 “Probing the Dark Energy through an Extremely Wide & Deep Survey with Subaru Telescope”, by World Premier International Research Center Initiative (WPI Initiative), MEXT, Japan, and by the FIRST program “Subaru Measurements of Images and Redshifts (SuMIRE)”. GPS acknowledges support from the Royal Society. KU acknowledges partial support from the National Science Council of Taiwan (grant NSC100-2112-M-001-008-MY3) and from the Academia Sinica Career Development Award.

REFERENCES

- Applegate, D. E., von der Linden, A., Kelly, P. L., et al. 2012, ArXiv e-prints
- Bahé, Y. M., McCarthy, I. G., & King, L. J. 2012, MNRAS, 421, 1073
- Bhattacharya, S., Habib, S., Heitmann, K., & Vikhlinin, A. 2011, ArXiv e-prints
- Böhringer, H., Schuecker, P., Guzzo, L., et al. 2004, A&A, 425, 367
- Broadhurst, T., Takada, M., Umetsu, K., et al. 2005, ApJ, 619, L143
- Broadhurst, T., Umetsu, K., Medezinski, E., Oguri, M., & Rephaeli, Y. 2008, ApJ, 685, L9
- Bullock, J. S., Kolatt, T. S., Sigad, Y., et al. 2001, MNRAS, 321, 559
- Dahle, H., Hannestad, S., & Sommer-Larsen, J. 2003, ApJ, 588, L73
- De Boni, C., Ettori, S., Dolag, K., & Moscardini, L. 2012, ArXiv e-prints
- Dolag, K., Bartelmann, M., Perrotta, F., et al. 2004, A&A, 416, 853
- Duffy, A. R., Schaye, J., Kay, S. T., & Dalla Vecchia, C. 2008, MNRAS, 390, L64
- Ebeling, H., Edge, A. C., Allen, S. W., et al. 2000, MNRAS, 318, 333
- Ebeling, H., Edge, A. C., Böhringer, H., et al. 1998, MNRAS, 301, 881
- Eisenstein, D. J., Weinberg, D. H., Agol, E., et al. 2011, AJ, 142, 72
- Einasto, J. 1965, Trudy Astrofizicheskogo Instituta Alma-Ata, 5, 87
- Gao, L., Navarro, J. F., Frenk, C. S., et al. 2012, MNRAS, 425, 2169
- Gavazzi, R., Fort, B., Mellier, Y., Pelló, R., & Dantel-Fort, M. 2003, A&A, 403, 11
- Gnedin, O. Y., Kravtsov, A. V., Klypin, A. A., & Nagai, D. 2004, ApJ, 616, 16
- Heymans, C., Van Waerbeke, L., Bacon, D., et al. 2006, MNRAS, 368, 1323
- Hoekstra, H. 2003, MNRAS, 339, 1155
- Hoekstra, H., Hartlap, J., Hilbert, S., & van Uitert, E. 2011, MNRAS, 412, 2095
- Ilbert, O., Capak, P., Salvato, M., et al. 2009, ApJ, 690, 1236
- Johnston, D. E., Sheldon, E. S., Wechsler, R. H., et al. 2007, ArXiv e-prints
- Kaiser, N., & Squires, G. 1993, ApJ, 404, 441
- Kaiser, N., Squires, G., & Broadhurst, T. 1995, ApJ, 449, 460
- Kneib, J.-P., & Natarajan, P. 2011, A&A Rev., 19, 47
- Kneib, J.-P., Hudelot, P., Ellis, R. S., et al. 2003, ApJ, 598, 804
- Komatsu, E., Smith, K. M., Dunkley, J., et al. 2011, ApJS, 192, 18
- Limousin, M., Richard, J., Jullo, E., et al. 2007, ApJ, 668, 643
- Mandelbaum, R., Seljak, U., Cool, R. J., et al. 2006, MNRAS, 372, 758
- McCarthy, I. G., Schaye, J., Bower, R. G., et al. 2011, MNRAS, 412, 1965
- Miralda-Escude, J. 1995, ApJ, 438, 514

- Miyazaki, S., Komiyama, Y., Sekiguchi, M., et al. 2002, PASJ, 54, 833
- Navarro, J. F., Frenk, C. S., & White, S. D. M. 1997, ApJ, 490, 493
- Navarro, J. F., Hayashi, E., Power, C., et al. 2004, MNRAS, 349, 1039
- Neto, A. F., Gao, L., Bett, P., et al. 2007, MNRAS, 381, 1450
- Newman, A. B., Treu, T., Ellis, R. S., et al. 2013, ApJ, 765, 24
- Oguri, M. 2010, PASJ, 62, 1017
- Oguri, M., Bayliss, M. B., Dahle, H., et al. 2012, MNRAS, 420, 3213
- Oguri, M., & Takada, M. 2011, Phys. Rev. D, 83, 023008
- Oguri, M., Hennawi, J. F., Gladders, M. D., et al. 2009, ApJ, 699, 1038
- Okabe, N., Takada, M., Umetsu, K., Futamase, T., & Smith, G. P. 2010, PASJ, 62, 811
- Okura, Y., & Futamase, T. 2012, ApJ, 748, 112
- Planck Collaboration, Ade, P. A. R., Aghanim, N., et al. 2013, A&A, 550, A129
- Popesso, P., Biviano, A., Böhringer, H., Romaniello, M., & Voges, W. 2005, A&A, 433, 431
- Sand, D. J., Treu, T., Smith, G. P., & Ellis, R. S. 2004, ApJ, 604, 88
- Smith, G. P., Kneib, J.-P., Ebeling, H., Czoske, O., & Smail, I. 2001, ApJ, 552, 493
- Smith, R. E., Peacock, J. A., Jenkins, A., et al. 2003, MNRAS, 341, 1311
- Umetsu, K., Broadhurst, T., Zitrin, A., et al. 2011, ApJ, 738, 41
- Umetsu, K., Medezinski, E., Broadhurst, T., et al. 2010, ApJ, 714, 1470
- Zhao, D. H., Jing, Y. P., Mo, H. J., & Börner, G. 2009, ApJ, 707, 354